Hydrol. Earth Syst. Sci. Discuss., 9, 7639–7697, 2012
www.hydrol-earth-syst-sci-discuss.net/9/7639/2012/
doi:10.5194/hessd-9-7639-2012

Hydrology and Earth System Sciences Discussions

Continuum: a distributed hydrological model for water management and flood forecasting

F. Silvestro[1], S. Gabellani[1], F. Delogu[1], R. Rudari[1], and G. Boni[1,2]

[1]CIMA Research Foundation, Savona, Italy
[2]DIST, University of Genova, Genova, Italy

Received: 24 May 2012 – Accepted: 1 June 2012 – Published: 14 June 2012

Correspondence to: F. Silvestro (francesco.silvestro@cimafoundation.org)

Published by Copernicus Publications on behalf of the European Geosciences Union.

Abstract

Full process description and distributed hydrological models are very useful tools in hydrology as they can be applied in different contexts and for a wide range of aims such as flood and drought forecasting, water management, prediction of impact on the hydrologic cycle due to natural and human changes to catchment features in present and changing climates. Since they must mimic a variety of physical processes they can be very complex and with a high degree of parameterization. This complexity can be increased by the need to relate the state variables to observations in order to allow data assimilation.

In this work a model, aiming at balancing the need to reproduce the physical processes with the practical goal of avoiding over-parameterization, is presented. The model is designed to be implemented in different contexts with a special focus on data scarce environments.

All the main hydrological phenomena are modeled in a distributed way. Mass balance and energy balance are solved explicitly. Land surface temperature, which is particularly suited to being extensively observed and assimilated, is an explicit state variable.

An objective performance evaluation, based on both traditional and satellite derived data, is presented with a specific reference to the application in an Italian catchment. The model has been calibrated and validated using different data sets on two nested outlet sections and the capability of the model in reproducing both the stream-flow measurements and the land surface temperature retrieved by satellite measurements, has been investigated.

1 Introduction

Continuous streamflow simulation is of fundamental importance in the support of water management decisions (e.g. best use of water resources) and civil protection actions (e.g. flood and droughts mitigation actions) (Schlosser et al., 1997; Middelkoop et al.,

HESSD

9, 7639–7697, 2012

2001; Karsten et al., 2002; Bartholomes and Todini, 2005). These are only some examples of the huge variety of cases where continuous hydrological models have been applied. The application of models to different problems resulted in the development of a number of hydrological models, which sometimes showed very different characteristics (e.g. Beven, 1997; Todini and Ciarapica, 2001; Rigon et al., 2006).

Over recent decades computation capacity has developed exponentially, meanwhile, due to the progress of earth observation techniques, a large amount of territorial information (digital elevation models, land use, soil and vegetation parameters) has become readily available. As result of this, full process descriptions and distributed hydrological modeling, assisted by detailed catchment descriptions, has become feasible, leading to the improvement in the understanding and representation of both runoff formation and propagation dynamics (Winchell et al., 1998; Giannoni et al., 2000). Distributed modeling allows us to understand the role played by space and time rainfall distribution (Giannoni et al., 2003), by soil and vegetation heterogeneity, and by the drainage network structure (Downer et al., 2002; Giannoni et al., 2000, 2005).

Several hydrological models provide a full description of all hydrological processes so that they can provide a continuous simulation in support of specific tasks such as long-term water balances and flood forecasting. Some examples starting from the early 1970s can be cited: Sacramento model (Burnash et al., 1973; Burnash 1995), SHE (Abbott et al., 1986), RIBS (Garrote and Brass, 1995), CASC2D (Julien et al.,1995), TOPMODEL (Beven, 1997; Wang et. al., 2006), TOPKAPI (Todini and Ciarapica, 2001), Geotop (Rigon et al., 2006), MobiDIC (Campo et al., 2006). They can usually work in different regimes and simulate continuously the spatio-temporal evolution of the state of the catchment. The advantages of these types of models have been highlighted in various works (Bartholomes and Todini, 2005; Liu et al., 2005; Castelli et al., 2009).

The use of models capable of exploiting distributed information has consolidated, with the penalty of increasing the number of model parameters with the associated problem of reliably estimating them (Abbott et al., 1986; Beven, 1993; Madsen, 2000; Anderson et al., 2006).

HESSD
9, 7639–7697, 2012

Because of the detailed and complete description of the hydrological cycle, these advanced models are characterized by an abundant number of parameters, which need a detailed knowledge of the catchment to which they are applied. Some of them, such as those describing soil physics and land use, have a direct physical meaning, they can therefore be estimated on the basis of maps of catchment information and geophysical cartography; nevertheless, the scale of representation, the detail and the temporal updating of information often do not match requirements for the reliable estimation of these parameters. Furthermore, relationships between land information and model parameters are sometimes indirect and affected by great uncertainty, nullifying, in practical applications, the benefit of an accurate process description.

The presence of many parameters, in general, allows modellers to obtain good results in the calibration phase, because of the adaptation skills of the model; however, this leads to an increased probability of obtaining similar results with different parameters sets (Beven and Binley, 1992; Beven and Freer, 2001; Savenije, 2001). This limits the possibility of reliable parameter estimation, hampering the predicting abilities of the model. There are two ways to face this issue: develop a parsimonious model or increase the means of identifying parameters from available data. The design of the "Continuum" model is based on a combination of the above-mentioned strategies. On the one hand, special attention is paid to reducing, as much as possible, the parameterization of the physical processes so that land information can be used as a constraint to parameters calibration. This results in a simpler calibration, efficiently applicable in a data scarce environment. On the other hand, the model parsimony has to be compatible with the necessity for a detailed description of all the terms of the hydrological cycle. This results in an increased number of observables in the model state variables, in order to exploit the potential offered by today's remote sensing (R.S.).

In the last decade many advances in satellite data development and analysis for earth observation have been reached. R.S. provides inputs to the model (e.g. meteorological input, catchment description, vegetation characterization) or observation of the state variables (e.g. soil moisture, land surface temperature). It is therefore a

HESSD
9, 7639–7697, 2012

concern for new models to include prognostic equations of satellite observables so that they can be used in the calibration/validation phase, or so that they can be used as constraints in a Data Assimilation framework (Kumar et al., 2008). Previous studies (e.g. Winsemius et al., 2006) highlighted the necessity to use remote and/or independent data to constrain the model uncertainties and its parameterizations. Clearly, the capability of simulating variables that are observable is a critical advantage for complex models.

The Continuum model aims at an equilibrium between simplicity and rigorous physical modeling while maintaining comparable performances to existing models; the reduced complexity of the schematizations and the relatively small number of parameters leads to a considerably lower calibration effort, increasing model robustness and portability to data scarce environments. The resulting increased computational efficiency leads to an easier utilization of the model in ensemble mode so that a direct quantification of prediction uncertainties is possible.

The article is organized as follows. In chapter two the components of the model are presented, chapter three describes the model's sensitivity analysis, the case study, as well as the parameters calibration and model's validation; chapter four contains discussion and conclusions.

2 Model description

Continuum is a continuous distributed hydrological model that strongly relies on a morphological approach, based on a novel way for the drainage network components identification (Giannoni et al., 2005).

The basin is represented using a regular square mesh based on Digital Elevation Model (DEM), the flow directions are identified on the basis of the directions of maximum slope derived by the DEM. The drainage network is represented distinguishing between hillslope and channeled flow. Distinction between hillslopes and channels is made with a filter defined by the expression $AS^k = C$ where A is the contributing area

HESSD
9, 7639–7697, 2012

upslope each cell (l^2) and S the local slope (–) (Giannoni et al., 2000). This is able to describe hydrodynamic and morphological conditions in the channeled network (Giannoni et al., 2000). The exponent k (–) is a function of the morphologic environment in which the network developed and weights the importance between flow accumulation and slope in determining active channeled flow (Giannoni et al., 2000). In mature morphological environments k can be set equal to 1.7 (Giannoni et al., 2000, 2003) while the threshold C can be calibrated following channel routing (Giannoni et al., 2005) and reproducing topographic independent information like the so called "blue lines". The identification of a drainage network and the classification of each cell as a channel or hillslope are the main concepts that have been maintained from the original model.

Infiltration and subsurface flow is described using a semi-empirical, but quite detailed, methodology based on a modification of Horton algorithm (Bauer, 1974; Disikin and Nazimov, 1997) and focuses especially onto exploiting land use information and climatology to set the infiltration parameters (see for details, Gabellani et al., 2008). The energy balance is based on the so-called "force restore equation" (Dickinson, 1988) which balances forcing and restoring terms, with explicit soil surface temperature prognostic computation. The overland runoff is distributed with differentiation between hillslope and channel flow. Vegetation interception and water table flow have been also schematized. The different approaches are detailed in the following paragraphs.

2.1 Overland and channel flow

The surface flow schematization distinguishes between channel and hillslope flow. In channels the momentum equation per unit of width is derived from the kinematic schematization (Wooding, 1965; Todini and Ciarapica, 2001), and it is expressed by the following equation:

$$q = u_c \cdot \sqrt{tg(\beta)} \cdot h^a \quad (1)$$

HESSD
9, 7639–7697, 2012

where q is the flow per unit of width ($l^2 t^{-1}$), u_c is a friction coefficient ($l^{(2-a)} t^{-1}$), $tg(\beta)$ is the surface local slope in channels, h is the depth of the flow in the channel (l). The exponent a is similar to the Manning's equation one. In general it varies between 1 and 5/3 (Marchi e Rubatta, 1981). We set $a = 1.5$ as representative of a mean behaviour. This choice is also consistent with the Darcy-Weisbach formulation in case of turbulent flow (Chow, 1959).

$tg(\beta)$ is a downstream averaged local slope, evaluated as a mean slope of a branch of length d^* downstream the actual pixel. It is estimated for the ith cell as:

$$tg(\beta_i) = \frac{1}{d^*} \sum_{j=1}^{n} \frac{z_i - z_j}{j} \tag{2}$$

where d^* is a reference maximum distance from the analyzed cell that varies around 1000–2000 m and $n = d^*/\Delta x$ where Δx is the cell size of the DEM (for the application presented in the following paragraphs $\Delta x = 100$ m). z_j is the level at a distance $j \cdot \Delta x$ (l). This smoothed slope reduces the impact of local DEM errors and inconsistencies.

The water depth for the i-th cell is evaluated combining the momentum equation and the mass balance equation (Liu et al., 2005):

$$\frac{\mathrm{d}h_i}{\mathrm{d}t} = I_i - \frac{1}{\Delta x} \cdot u_c \cdot \sqrt{tg(\beta_i)} \cdot h_i^{1.5} \tag{3}$$

where I_i represents the input per unit of area (the sum of runoff, saturation excess and inflow discharge from upstream) to the grid cell ($l t^{-1}$).

On the hillslopes the overland flow has a linear equation for the motion:

$$q = \Delta x \cdot u_h \cdot h_i \tag{4}$$

where u_h parameterizes the main morphologic characteristics of the hillslopes (t^{-1}) (slope, roughness, etc.). The final schematization collapses into a linear reservoir model.

HESSD
9, 7639–7697, 2012

The parameters u_h and u_c need calibration at basin scale.

In both hillslopes and channels the re-infiltration process is accounted for: the input to the ith cell must exceed its infiltration capacity, otherwise it infiltrates into the soil.

2.2 Vegetation interception

Interception includes the portion of rainfall that is caught by tree leaves, grass and vegetation cover in general, and is evaporated before it touches the ground. Ponding effects are also included in this initial abstraction. Interception is modeled by a simple empirical equation similar to the one used by Rey (1999), Kozak et al. (2007), Zhao (2003), among others. A maximum retention capacity S_v is introduced, and it is estimated as a function of the Leaf Area Index (LAI) by the relationship (Kozak et al., 2007):

$$S_v = 0.95 + 0.5 \cdot \mathrm{LAI} - 0.06 \cdot \mathrm{LAI}^2 \quad \text{(I)}. \tag{5}$$

The water in the reservoir with capacity S_v is evaporated at the potential rate without affecting the infiltration computation; the input is the precipitation (see Fig. 1). The advantage of using a LAI dependent expression is that the model takes into account vegetation variability in space and time. LAI is usually updated every 15 days from satellite optical sensors data.

2.3 Infiltration and subsurface flow

The infiltration methodology is a modification of the Horton equation (Diskin and Nazimov, 1994; Gabellani et al., 2008) based on physically interpretable parameters and accounts for soil moisture evolution even in condition of intermittent and low-intensity rainfall (namely lower than the infiltration capacity of the soil $f(t)$ when the filter is applied).

HESSD
9, 7639–7697, 2012

The soil is schematized as a reservoir with capacity V_{max} (l) and a selective filter $g(t)$ (lt^{-1}) manages the inflow:

$$g(t) = f_0 + (f_1 - f_0) \cdot \frac{V(t)}{V_{max}} \tag{6}$$

where f_0 is the initial infiltration rate and f_1 is the final infiltration rate considered as a function of f_0 (Mishra and Singh 2003):

$$f_1 = c_f f_0. \tag{7}$$

The method proposed by Gabellani et al. (2008) has been further modified by introducing the field capacity of the soil, defined as the water content that can be held by capillarity against the force of gravity, as:

$$V_{fc} = c_t V_{max} \tag{8}$$

with the parameter $c_t \in [0, 1]$. In this new configuration (see Fig. 1) the dynamic mass-balance equation for the soil can be written for each cell as:

$$\frac{dV}{dt} = g(t) - r_p(t) \tag{9}$$

with:

$$r_p(t) = f_1 \frac{V(t) - c_t V_{max}}{V_{max}(1 - c_t)}. \tag{10}$$

The input $r_1(t)$ is obtained by the sum of the effective rain (rain depleted by vegetation interception) and of the upstream overland flow, this allows the model to asses the re-infiltration. If $r_1(t)$ is less than or equal to $g(t)$ there are the first two cases:

HESSD
9, 7639–7697, 2012

$$V(t) \le c_t V_{max} \qquad \frac{dV}{dt} = r_1(t) \tag{11}$$

$$V(t) > c_t V_{max} \qquad \frac{dV}{dt} = r_1(t) - f_1 \frac{V(t) - c_t V_{max}}{V_{max}(1 - c_t)}. \tag{12}$$

If $r_1(t)$ is greater than $g(t)$:

$$V(t) \le c_t V_{max} \qquad \frac{dV}{dt} = f_0 + (f_1 - f_0) \cdot \frac{V(t)}{V_{max}} \tag{13}$$

$$V(t) > c_t V_{max} \qquad \frac{dV}{dt} = f_0 + (f_1 - f_0) \cdot \frac{V(t)}{V_{max}} - f_1 \frac{V(t) - c_t V_{max}}{V_{max}(1 - c_t)}. \tag{14}$$

The runoff $r_2(t)$ is:

$$r_1(t) > g(t) \qquad r_2(t) = r_1(t) - g(t) \tag{15}$$

$$r_1(t) \le g(t) \qquad r_2(t) = 0. \tag{16}$$

The infiltration scheme has four parameters: the initial infiltration rate f_0, the maximum soil retention capacity V_{max}, and the parameters to define soil field capacity c_t and final infiltration rate c_f. The parameters f_0 and V_{max} are related to the soil type and land use through the Curve Number (CN) parameter (Risse et al., 1995). Following Gabellani et al. (2008) they can be easily derived by soil use and soil type maps. c_t and c_f are calibration parameters and are assumed to be constant for the whole basin as the pattern of f_1 and V_{fc} is modulated by the pattern of V_{max}. If detailed basin information, soil parameters or other kind of data were available it would be possible to follow a different approach for f_0 and V_{max} estimation by obtaining them from physical soil attributes.

The percolation rate separates into two components: a contribution to subsurface flow r_{Hy} and one to deep flow r_d or recharging water table defined as:

$$\begin{aligned} r_{Hy} &= \sin\alpha \cdot r_p(t) \\ r_d &= (1 - \sin\alpha) \cdot r_p(t) \end{aligned} \tag{17}$$

HESSD
9, 7639–7697, 2012

where the angle α is such that $tg(\alpha)$ is the downslope index as in Hjerdt et al. (2004); $\sin(\alpha)$ is a decomposition term that increases with the terrain slope, reproducing the major proneness of the high slope areas to subsurface flow due to gravity. We decided to use the downslope index instead of the more commonly used topographic slope estimated with the local gradient for various reasons: first, it seems to be less sensitive than local surface slope to changes in DEM resolution (Hjerdt et al., 2004), second, it is less affected by local discontinuities and errors of the DEM, and finally, it is able to capture dominant controls on local drainage regimes, especially in cases where profile curvature exerts a strong control on the drainage pattern (see Hjerdt et al., 2004 for details).

The subsurface flow is propagated between cells following the surface drainage network directions and the soil moisture state of each cell is updated by considering both the infiltration, estimated by the modified Horton method, and the inflow from the upper cells. Therefore a cell can reach saturation because of the percolation from upper cells causing saturation excess (Dunne and Black, 1970).

The coupling between the infiltration model and the schematization of subsurface flow is quite simple and it gives a good conceptualization of the physical processes involved. The small number of calibration parameters confers robustness to the model. This mass balance approach provides a good representation of the time evolution of soil moisture spatial patterns.

In Fig. 1 the sketches of vegetation retention and subsurface flow at cell scale are presented.

2.4 Deep flow and water table

Several approaches are possible to describe the dynamics of both the deep flow and the water table, with examples from Darcy's law applications to conceptual reservoir models (Todini and Ciarapica, 2001; Rigon et al., 2006; Campo et al., 2006). However, it is often difficult to have the data necessary for the correct implementation and parameterization of water table dynamics (Castelli et al., 2009).

HESSD
9, 7639–7697, 2012

In Continuum the water table evolution is modeled with a simplified approach, with the objective of reducing the need for external data and the number of parameters, but maintaining a physical and distributed description of the process. Above all we are interested in the water table interaction with soil surface and to its effects on surface flow and soil moisture spatial pattern.

The soil is schematized as a unique homogeneous layer above the lower boundary containing the aquifer. The thickness of this layer is expressed in terms of maximum volume of water content of the aquifer and it is estimated by following Saulnier et al. (1997) using the surface slope as a proxy. The maximum water content in every cell (i) of the basin is given by:

$$V_{\mathrm{Wm}i} = V_{\mathrm{Wmax}} \cdot \left(\frac{tg(\alpha_{\max}) - tg(\alpha_i)}{tg(\alpha_{\max}) - tg(\alpha_{\min})}\right) \tag{18}$$

where V_{Wmax} is the absolute maximum water content of the aquifer on the whole investigated area; this sets a limit that is basically a calibration parameter (see Fig. 2).

The reservoir is fed with r_{d} (see previous paragraph).

The water table level is then:

$$h_{\mathrm{W}i}(t) = z_i - \frac{V_{\mathrm{Wm}i} - V_{\mathrm{W}i}(t)}{\eta} \tag{19}$$

where z_i is the elevation of the ith cell, η is the soil porosity and $V_{\mathrm{W}i}(t)$ the actual water content.

In the model, the equation is simplified assuming uniform soil porosity so that Eq. (19) becomes

$$h_{\mathrm{W}i}(t) = z_i - V_{\mathrm{Wm}i} + V_{\mathrm{W}i}(t). \tag{20}$$

And the effect of porosity is considered as a multiplicative factor in the Darcy equation used to estimate the flux per unit area between two contiguous cells (i and j):

$$q_{ij} = \frac{h_{\mathrm{W}i} - h_{\mathrm{W}j}}{\Delta x} \cdot R_{\mathrm{f}} \cdot f_{1i} \tag{21}$$

HESSD
9, 7639–7697, 2012

where Δx is the DEM spatial resolution and f_{1_i} is the final infiltration rate estimated as in Eq. (7) and R_f is the above mentioned factor which also takes care of differentiating the saturated vertical and horizontal conductivity.

Each cell can drain towards all the neighboring cells following the 2-D water table gradient that depends on the elevation and on the water content of each cell.

When the water table reaches the surface ($V_{Wi}(t) = V_{Wmi}$), the deep percolation term in Eq. (17) is inhibited. While the condition $V_W(t) \cong 0$ is a limit that can only be reached after a very long and anomalous dry period. This doesn't mean that in deepest soil layers there is no water (in particular in flat areas), simply in this context, the model neglects this contribution.

The proposed scheme is a quite coarse simplification of the process, but it implements a distributed interaction between the water table and the subsurface flow and is proved to efficiently reproduce the base flow far from rainfall events with a parsimonious parameterization. Only the absolute maximum water content should be estimated and the ratio between the saturated vertical and horizontal conductivity at catchment scale needs to be set.

2.5 Energy balance and evapotranspiration

The representation of surface mass and energy turbulent fluxes requires the solution of a conservation equation for mass and energy (Deardorff, 1978) driven by temperature and moisture content. Since the vertical gradient of such variables is quite large, a high-resolution multiple layer model would be required to estimate soil surface temperature and moisture content with accuracy. Such an approach demands substantial amounts of computing resources to solve the balance equations. An alternative approach makes use of computationally efficient parameterization of soil heat and moisture flux terms. Bhumralkar (1975) and Blackadar (1976) independently showed that the heat flux into the soil could be parameterized by the sum of a temperature-derivative term and the difference between ground surface and deep soil temperature. Deardorff (1978) referred to this approach as the "force-restore" method because the forcing by net radiation is

HESSD
9, 7639–7697, 2012

modified by a restoring term that contains the deep soil temperature. Lin (1980) demonstrated that the predicted ground surface temperature by the "force-restore" method performed well compared with the field-measured temperature. Since then the "force-restore" method has been widely used in land surface modeling (e.g. Dickinson, 1988; Dickinson et al., 1993; Noihan and Planton, 1989; Caparrini et al., 2004). The force-restore equation essentially reduces the partial differential equation of heat diffusion into an ordinary differential equation for the ground surface temperature of a soil slab of thickness δ (Hu and Islam, 1995). Hu and Islam (1995) demonstrated that the force restore equation is the solution of the heat diffusion equation, with purely sinusoidal forcing assuming that the thermal properties are constant with depth and the surface forcing term is also nearly independent of air temperature and has a strong periodic behavior in time.

The Continuum model solves a complete and explicit energy balance by using the force restore approach for land surface temperature (Dickinson, 1988). The conservation of energy at soil surface is given by:

$$G = R_n - H - \mathrm{LE} \tag{22}$$

where R_n is the net radiation, H is the sensible heat flux, LE the latent heat flux and G the ground flux (all in $\mathrm{E\,t^{-1}\,l^{-2}}$).

The daily cycle of land surface temperature (LST) has the implicit signature of the energy balance. Maximum amplitudes of LST diurnal cycle are usually reached in the presence of bare and dry soil. The presence of moisture on the surface and in the subsurface soil greatly moderates the daily range of LST. The vegetation cover has a similar effect. The force restore approach leads to the following equation for LST:

$$\frac{\mathrm{dLST}}{\mathrm{d}t} = 2 \cdot \sqrt{\pi\omega}\left(\frac{R_n - H - \mathrm{LE}}{\phi}\right) - 2\pi\omega \cdot (\mathrm{LST} - T_{\mathrm{deep}}) \tag{23}$$

where ϕ ($\mathrm{E\,l^{-2}\,T^{-1}\,t^{-(1/2)}}$) is the effective thermal inertia and T_{deep} (T) is a "restoring" deep ground temperature. T_{deep} is evaluated by filtering data for air temperature at

HESSD
9, 7639–7697, 2012

ground level (Caparrini et al., 2003, Caparrini and Castelli, 2004). Thermal inertia is a function of conductivity, density and specific heat capacity of soil and it is evaluated with the following equation:

$$\phi = \sqrt{C_{\text{soil}} \cdot K_{\text{soil}}} \tag{24}$$

where C_{soil} ($\text{E}\,\text{T}^{-1}\,\text{l}^{-3}$) is the soil heat capacity and K_{soil} ($\text{E}\,\text{t}^{-1}\,\text{l}^{-1}\,\text{T}^{-1}$) is the soil thermal conductivity. Both the terms depend on the soil characteristics and they are estimated as proposed in Peters et al. (1997). C_{soil} and K_{soil} also depend on soil saturation degree θ consequently they vary in time.

The turbulent sensible heat flux is estimated using a bulk transfer approach based on bulk transfer formula (Deardoff, 1968):

$$H = \rho \cdot c_{\text{p\_air}} \cdot C_{\text{H}} \cdot U \cdot (\text{LST} - T_{\text{a}}) \tag{25}$$

where $c_{\text{p\_air}}$ ($\text{E}\,\text{m}^{-1}\,\text{T}^{-1}$) is the specific heat of air, ρ ($\text{m}\,\text{l}^{-3}$) the air density, C_{H} (–) the bulk transfer coefficient for heat, U ($\text{l}\,\text{t}^{-1}$) is the wind velocity and T_{a} (T) is the air temperature at reference elevation.

The latent heat flux is defined as:

$$\text{LE} = \rho \cdot \lambda_{\text{LE}} \cdot C_{\text{E}} \cdot U \cdot \beta_{\text{f}} \cdot (e_{\text{s}}^{*} - e_{\text{a}}) \cdot 0.622 \cdot \frac{1}{P} \tag{26}$$

where λ_{LE} ($\text{E}\,\text{m}^{-1}$) is the latent heat of vaporization, $(e_{\text{s}}^{*} - e_{\text{a}})$ ($\text{m}\,\text{t}^{-2}\,\text{l}^{-1}$) the difference in vapor pressure between the surface (at saturation) and air at reference elevation, C_{E} (–) is the bulk transfer coefficient for moisture, β_{f} (–) is a coefficient proportional to the first soil layer saturation degree as described in Castelli (1995) and P ($\text{m}\,\text{t}^{-2}\,\text{l}^{-1}$) is the atmospheric pressure.

The bulk transfer coefficient for heat and moisture can be estimated using empirical formulations (Deardoff, 1968) or could be yield by other models (Caparrini and Castelli, 2004). C_{H} (–) effectively represents the role of vegetation in the energy balance.

HESSD
9, 7639–7697, 2012

The choice of the so-called "force-restore" equation for LST dynamics is based on the fact that it can be numerically implemented with a limited effort. Furthermore the equation input variables are commonly observed by ground based micrometeorological networks. Since remote sensors can estimate LST the explicit description of its dynamics allows Continuum to be used in a data assimilation framework. The soil parameters used in the estimation of the thermal inertia, usually constant at basin scale, can be estimated by a data assimilation process, or related to soil type (Peters et al., 1997) when reliable maps are available.

In Continuum the evapotranspiration ET ($\mathrm{m\,s^{-1}}$) is estimated as:

$$\mathrm{ET} = \frac{\mathrm{LE}}{\rho_{\mathrm{w}} \cdot \lambda_{\mathrm{LE}}} \tag{27}$$

where ρ_{w} ($\mathrm{ml^{-3}}$) is the water density. ET is deducted from the subsurface reservoir $V(t)$.

2.6 Model summary

In summary, Continuum is a distributed model based on a space-filling representation of the network, directly derived from a DEM. The DEM resolution coincides with the model resolution. The mass and energy balances are solved at cell scale referring to the schematizations of subsurface flow, deep flow and vegetation interception. The overland and channel flow are described by a linear and a non-linear tank schematization, respectively.

Figure 3 is a sketch of the Continuum structure. Two consecutive cells are considered to highlight the interaction between the single modules.

Continuum can work with different time steps (Δt_{m}), generally smaller than 1 day. Time steps, in the range between 10 min to 1 h, are appropriate when the objective is a flood simulation, and they are consistent with commonly available meteorological data. The overland and channel flow module works with a time step (Δt_{s}) that is

HESSD
9, 7639–7697, 2012

smaller than Δt_m because of problems of numerical stability and it depends on the DEM resolution.

The main characteristics of the presented model and its advantages with respect to most of the existing models can be summarized as follows:

- a reduced number of land data is needed for the implementation (DEM and CN maps are the essential information needed);
- there are a reduced number of calibration parameters reducing the problem of parameter evaluation, most of the parameters can be evaluated by means of independent information (e.g. morphologic information, climatic information, soil information) without using input-output time series;
- the capability of exploiting the possibilities offered by remote sensing (e.g. satellite data, better clarified in the following sections) smoothing the problem of equifinality by increasing the model's constraints;
- the capability of modeling a large number of state variables, similarly to more complex models.

Six model parameters need calibration on the basis of input-output time series: c_f, c_t, u_h, u_c, R_f, V_{Wmax} (see Table 1). The first two parameters c_f, and c_t mainly rule the generation of runoff and the movement of water in the different soil layers, while u_h and u_c control the surface water motion, V_{Wmax} represents the maximum storage capacity of the aquifer and R_f summarizes the effect of soil porosity as well as of the ratio between vertical and horizontal saturated soil conductivity.

HESSD
9, 7639–7697, 2012

3 Case study: Orba watershed

3.1 Watershed description

The model has been tested on the Orba basin located in the southern part of the Piemonte region in the Apennine (see Fig. 4). The Orba River originates from Mt. Reixa (1183 m a.s.l.) in the Beigua Massif and it flows into the Bormida River, a tributary of the Tanaro River, before it reaches the town of Alessandria. Three main morphological areas can be identified: a mountain part characterized by very steep sub-catchments with a very deep river bed, a mild part with an average slope of 1 %, and finally the alluvial part characterized by very small slope values. The Orba River has mainly a torrential regime with recurrent flash floods during the autumnal and spring rainfall seasons and very low flows during summer. The Orba mean annual flow in correspondence of the confluence with Bormida River is around 20 $m^3 s^{-1}$.

3.2 Dataset

The micrometeorological networks of Liguria and Piemonte Italian Regions provide meteorological inputs. In the Orba basin there are 31 rain gauges, 27 thermometers, 6 hygrometers, 4 radiometers (shortwave) and 4 anemometers. The temporal resolution of the observations is one hour. This latter is also the temporal resolution used in the model application (Δt_m = 1 h). The overland and channel flow module uses Δt_s = 30 s.

Observations from two nested stage discharge gauges, with reliable and constantly updated discharge rating curves, are used for model calibration and validation (Fig. 4). The Tiglieto station (75 km^2) is located in the upper part of the basin, characterized by a mountainous morphology with high slopes, and a high percentage of the territory is covered by forest. The Casalcermelli station drains an area of 800 km^2 and it is placed in the final part of the basin in a quite flat environment. This allows for the testing of the model on different spatial and temporal scales over the same basin.

HESSD
9, 7639–7697, 2012

Two different periods have been simulated: the calibration period starts from 1 June 2006 and ends on 31 December 2006, while the validation period starts from 1 June 2009 and ends on 31 December 2009. No significant snowfall and accumulation were observed during both periods.

DEM and CN maps with spatial resolution equal to 100 m are available for the basin. $\Delta x = 100$ m is assumed as the model grid size. LAI maps have been produced with temporal update of fifteen days as averaged values of daily maps obtained by Meteosat Second Generation. The LAI product is based on the information provided by the three short-wave channels of MSG-SEVIRI (VIS 0.6 µm, NIR 0.8 µm, SWIR 1.6 µm), which are used to derive the fractional vegetation cover (FVC) product (EUMETSAT, 2008). The spatial resolution is about 0.04° (about 4.5 km). The time resolution of MSG allows us to have cloud free estimations of LAI on the area.

3.3 Sensitivity of calibration parameters

A set of simulations has been carried out to evaluate the effects on the simulated hydrographs of the calibration parameters shown in Table 1.

The parameters u_c and u_h impact the water flow on the surface. High values of these two parameters lead to narrow and highly peaked hydrographs. u_h has influence on the general shape of the hydrograph while u_c has an increasing influence with the increasing length of the channeled paths (e.g. large/elongated basins), it modifies the peak flow value as well as the peak arrival time.

The sensitivity analysis of parameters u_h and u_c has been made considering a short period of simulation (16 to 18 August 2006) since they influence directly the overland flow. The first subplot of Fig. 5 shows that u_h has a considerable influence on both the Tiglieto and Casalcermelli outlets. The peak values and the hydrographs shape have quite a large range of variation, while peak times are not significantly affected by this parameter.

The second subplot of Fig. 5 shows the influence of u_c. It mainly affects the shape and the peak times on the Casalcermelli outlet section while hydrographs of the Tiglieto

HESSD
9, 7639–7697, 2012

outlet shows negligible differences. Note that Casalcermelli has a drainage area that is one order of magnitude larger in respect to Tiglieto.

The parameter c_t is related to the soil field capacity and defines the fraction of water volume in the soil not available for percolation and subsurface flow. It has an impact on the dynamics of soil saturation between rain events: higher values of c_t reduce the soil drying time scale especially during the cold season, with consequent higher runoff coefficients for single rainfall events. However, the subsurface flow tends to vanish rapidly because water level drops easily under the field capacity.

The parameter c_f controls both the velocity of subsurface flow and the dynamics of saturation of the single cells. Low values of c_f (i.e. low values saturated hydraulic conductivity) tend to cause the rapid saturation during rainfall events associated with slow subsurface flow increasing runoff production. Higher values of c_f produce a rapid subsurface flow with saturated areas that quickly concentrate along the drainage network.

Considering the common values for soil field capacity and soil hydraulic conductivity (Maidment, 1992; Dingman 1994) reasonable ranges for c_t and c_f are $0.2 < c_t < 0.6$ and $0.01 < c_f < 0.1$.

The combination of the two soil parameters c_t and c_f controls the distribution of the volumes of soil and surface water in space and time and it impacts soil humidity propagation. c_t and c_f influence the mass balance over long periods and regulate the exchanges between subsurface flow and runoff. We tested their influence simulating all the calibration period and analyzing the changes of the hydrographs for the last flood event; the figures cover the period between 7 and 10 December 2006. The third and fourth panels in Fig. 5 show how they affect the tails of the hydrographs and the values of peak flows. The effect of the combination of these two parameters is quite complex and it is only partially represented in the figures, they must be calibrated over long periods of time, using at best, external soil information when available.

The parameter R_f regulates the response of the deep flow and mainly influences low flow regimes while for larger basins it also affects high discharges. In Fig. 6 the period between 14 and 17 September 2006 is shown. The effects of R_f on the Tiglieto outlet

HESSD
9, 7639–7697, 2012

are negligible during the flood while the influence on low flows is more relevant for both the outlet sections.

Particular remarks need to be made about V_{Wmax}: a measure of the capacity of the basin for storing water in its aquifer and deep soil layer.

It is not easy to define a value for V_{Wmax} that reproduces a correct or realistic distribution of the deep soil layer water storage throughout the basin due to the fact that this distribution is hard to observe. Tests made using different values of V_{Wmax} in a physically acceptable range and starting from the same initial condition show that the model has low sensitivity to this parameter when the period of simulation covers between 6–12 months. This is related to the slow temporal dynamic of the water table. If data series for very long simulations (many years) are available the parameter V_{Wmax} can be re-calibrated and adjusted.

In the adopted scheme the initialization of the related state variable $V_W(t)$ is more important than its upper limit. In fact, practice demonstrates that the definition of the water table initial condition $V_W(t = 0)$ evidently influences simulated discharge. A reasonable initial condition produces a rapid stabilization of the water table with dynamics driven by the water input from upper soil layer. Two considerations are made in order to define these: (i) in correspondence of the drainage network the water table is generally next to soil surface because it is continuously recharged by the upstream portions of catchment, (ii) the mountainous parts of the water table receive reduced contribution because they drain small areas and are characterized by high gradients and here the water table has lower levels. Based on these considerations water table initial conditions are set as follows.

$V_W(t = 0)$ in correspondence of channels is set close to V_{Wmax}. In the hillslopes the level of $V_W(t = 0)$ is estimated supposing it inversely proportional to the downslope index α (Hjerdt et al., 2004).

All state variables need initial conditions but the sensitivity to this critical condition is reduced in a shorter warm-up period than for V_{Wmax}.

HESSD
9, 7639–7697, 2012

All these simulations highlighted another important feature of the model. Because of its internal structure it is possible to map different processes, and therefore different parts of the hydrograph, onto the parameters, so that different parts of the hydrograph's time series can be used separately to better identify model parameter values. Further analysis is needed to show sensitivity to spatial and temporal resolution. In addition a more detailed parameter uncertainty analysis will be carried out in a more specific work.

3.4 Calibration

The data set collected for the period 1 June to 31 December 2006 is particularly suitable for calibration under different hydrological conditions as it contains a range of significant floods and a preceding drought period. Runs of the model have been carried out for the whole year 2006, but the first five months are considered as model start up. This is to ensure that the initial conditions do not affect the results; in the Mediterranean climate the soil moisture and water table level at the beginning of the year are strongly related to the rain events that occurred during the previous autumn.

The first part of the calibration period is quite dry with an absence of precipitation for more than two months. A very intense and persistent event started on 16 August 2006 and lasted about 10 h with peak rainfall intensities larger than 70 mm h^{-1}. On 14 September 2006 another intense event with a 24 h duration and considerable rainfall accumulation took place.

For the calibration period we referred to empirical formulations that use wind speed and air temperature data to estimate the bulk transfer coefficient for heat and moisture (Deardoff, 1968). They do not account for vegetation variability.

Several skill estimators are considered in order to evaluate the performance of Continuum: Nash and Sutcliffe (1970), Chiew and McMahon (1994), correlation coefficient (CORR), root mean square error (RMSE) and percentage error on six flood events in the period. The first three estimators assume the value 1 if observation and simulation match 100 % while the other estimators tend to be 0 for a perfect simulation. The

HESSD
9, 7639–7697, 2012

parameters have been calibrated in order to maximize the Nash Sutcliffe coefficient, which is one of the most commonly used skill estimators in hydrology to compare observed and simulated hydrographs (Legates and McCabe, 1999).

$V_{W\max}$ has not been considered for calibration, it has been set to the value $V_{W\max}$ = 1500 mm.

The calibration has been performed in two steps. Initially, to reduce their range of variation, the two overland flow parameters have been calibrated on a short time period (16 to 18 August 2006). The errors on peak flow and on peak time on both the outlet sections have been minimized. Finally, a global calibration has been made including the three soil parameters c_t, c_f and R_f maximizing the Nash Sutcliffe coefficient. Table 2 reports the set of parameters obtained by the calibration procedure.

Table 3 shows the skill estimators calculated for the entire simulation; Table 4 reports the percentage errors on peaks flow (PPE) for the two outlet sections, Tiglieto and Casalcermelli.

Figures 7 and 8 report the simulated hydrographs compared with observations, we plot the entire simulation and the four most important events that occurred during the calibration period. The skill estimators' values synthesize the good performance of the model for both outlets and Figs. 7 and 8 highlight the capability of the model in reproducing the observed hydrographs in different discharge regimes.

3.5 Validation

Validation has been carried out during the period from 1 June 2009 to 31 December 2009. During the summer only a few precipitations occurred with negligible ground effects. Consistent rainfall events started in October and the most relevant occurred in November and December. Similarly to what was done for the model calibration a warm up period of five months has been considered and the simulation started 1 January 2009.

HESSD
9, 7639–7697, 2012

Continuum describes spatial and time evolution of LST by modeling the energy balance with a force restore approach as an approximation of the equation of heat diffusion in the soil.

The bulk transfer coefficient for heat C_H used in the energy balance equations is in general estimable by using empirical expressions which depend on wind speed, pressure and on vegetation characteristics that define the neutral transfer coefficient C_{HN}. The vegetation parameterization is often derived by literature values and it is considered constant in space and time because of the difficulty of evaluation in a real context. By using proper models that describe the vegetation and soil interaction with the atmosphere, it is possible to produce a more detailed C_{HN} estimation, that takes into account the vegetation spatial distribution and its seasonal variability. In this work the C_{HN} estimation is carried out using a variational assimilation scheme as described in Caparrini and Castelli (2004); maps of C_{HN} are produced every fifteen days for the entire validation period. The application of this model has been possible for the validation period only.

3.5.1 Streamflow validation

Table 5 reports the skill estimators for the whole validation period while Table 6 reports the percentage errors of the peaks of the main flood events.

Skill estimators assume similar or better values during validation period respect to the calibration period; this indicates the robustness of the model. Figures 9 and 10 report the simulated hydrographs compared with observations for the two outlet sections, as can be seen the model reproduces well the observed discharges. In particular, during the most important flood events, Continuum simulates the shape of the hydrograph the peak flows and the peak times surprisingly well.

HESSD
9, 7639–7697, 2012

3.5.2 Land surface temperature analysis

The LST estimated by Continuum have been compared with LST retrieved by satellite measurements. The database of LST estimations provided by LAND SAT application facility (SAF) of EUMETSAT has been used (EUMETSAT, 2009), land surface temperature estimations are available every fifteen minutes with a spatial resolution of about 0.04°. Data are available for the validation period only. The retrieval of LST (Freitas et al., 2010) is based on clear-sky measurements from the MSG system in the thermal infrared window (MSG/SEVIRI channels IR108 and IR120). The analysis has been carried out for the period 1 June 2009 to 31 December 2009.

Due to the complex topography of the Orba basin, the LST satellite estimates can not be directly compared to model outputs because of the following problems: (i) the georeferencing of model pixels and satellite pixels, (ii) the shadowing due to the presence of the mountains (iii) the variation of the satellite viewing angle for the different detected areas, (iv) the different spatial resolution (Satellite estimates spatial resolution is about 4.5 km while model output is about 0.1 km). A land application model (Fabio Castelli, personal communication, 2009) that projects the radiance obtained from the model (obtained from the simulated LST) to the same geometry of the satellite observations solve these 4 cited issues. The land application model produces a correlation matrix that weights the model radiance to estimate the portion of energy of each model pixel that contributes to the energy of the satellite pixel. The application of the land surface model can be formalized as:

$$\overline{\varepsilon_o} \cdot \overline{\mathrm{LST}_o^4} = \mathbf{M} \cdot \left(\overline{\varepsilon_m} \cdot \overline{\mathrm{LST}_m^4} \right) \tag{28}$$

where **M** is a matrix operator that weights the model output and maps it on the same grid of satellite data. ε_m and ε_o are the model and the satellite thermal emissivity, LST_m and LST_o are the modeled and the satellite estimates land surface temperatures. The model assumes a constant ε_m, and ε_o is estimated as the mean thermal emissivity of the two sensor channels used for LST-SAF retrieval.

HESSD
9, 7639–7697, 2012

We compared the basin mean LST and the LST of three selected pixels. The three pixels have been chosen from different areas of the basin to investigate the model behavior in different environments. One pixel is in the mountainous part of the basin (we name it Mountain Pixel), one is in the mid part (we name it Hill Pixel) and one is near the outlet section in the flood plain (we name it Flat Pixel).

Four skill estimators have been used to evaluate the performances of the model: the mean bias (BIAS), the root mean square error (RMSE), the mean absolute error (MAE) and the correlation coefficient (CORR).

Figures 11–14 report the scatter plot of satellite estimates and simulated LST for the mean basin comparison and for the pixels analysis.

The model slightly overestimates the LST during some periods of the warm season (Figs. 15 and 16), while slightly underestimates LST during the cold season, in particular during the central hours of the day. This behavior could be related to a slight overestimation of the model soil thermal inertia.

However, the general trends and diurnal cycle amplitude are well reproduced and the skill estimators' evidence shows quite a good performance (see Table 7); BIAS, RMSE, and MAE are quite small, while CORR is next to 1. The root mean square error of satellite LST estimation with respect to in situ measurements is about 2–3 °C (Freitas et al., 2010). The model reproduces well the trend and the daily periodicity of LST, Figs. 15 and 16.

Figure 17 shows satellite estimates and simulated LST plotted with the mean incoming solar radiation at basin scale for a period of a few days. The LST is strongly related to the radiation and the model is able to correctly reproduce the rapid changes in LST due to solar radiation variations.

The soil humidity is a factor that influences the thermal inertia and, as a consequence, the LST. We noted that, for example, the simulated LST overestimates the satellite estimates during a dry period at the beginning of summer (June–July), where Continuum produces very low values of soil humidity at basin scale. This can be related to the fact that AE and CORR are similar for all the target areas (Table 7), while BIAS

HESSD
9, 7639–7697, 2012

is higher and positive on Mountain Pixel where Continuum tends to dry the soil quickly because of the percolation and the soil humidity propagation. This behavior becomes evident in Fig. 18 that depicts the RMSE map of LST distributed in the catchment layered over the DEM relief. RMSE high values tend to concentrate in mountainous areas. Another interpretation of this result is that in such areas the variance of LST is higher due to altitude variation and this influences the statistics when aggregated at the MSG pixel size. However, we can deduce that a better LST simulation could be obtained by varying model parameters so as to obtain a different soil humidity distribution. Further analysis is needed to verify this hypothesis and it was not carried out in this study. It is, however, interesting to note that LST could be actually an additional constraint in the calibration phase.

4 Discussion and conclusions

The article describes a distributed and continuous hydrological model that balances the necessity for a complete description of hydrological cycle with a simple and versatile structure resulting in a small number of parameters. It has been designed for a variety of purposes: flood forecast and simulation, water resource management and droughts. The model is able to reproduce the spatial-temporal evolution of soil moisture, energy fluxes, surface soil temperature and evapotranspiration, moreover it can account for seasonal vegetation variability in terms of interception and evaporation. Deep flow and water table evolution are modeled with a simple scheme that reproduces the main physical characteristics of the process and a distributed interaction between water table and soil surface with a low level of parameterization.

The model has been conceived to be a compromise between models with a strong empirical connotation, which are easy to implement but far from reality, and complex physically based models which try to reproduce the hydrological processes with high detail but which introduce a hard parameterization and consequent uncertainty and lack of robust parameters identification.

HESSD
9, 7639–7697, 2012

The introduction of the so-called "force restore" equation for the surface energy balance, allows the LST estimation and makes the model feasible to exploit remote sensing data. These latter can be used for calibration or, more appropriately, in a data assimilation framework.

Referring to already tested calibration methodologies (Gabellani et al., 2008) and making some basic assumptions, the calibration task can be reduced to just six parameters at catchment scale. Consequently, the parameter space is really small for a distributed continuous model, and Continuum can be implemented with easily accessible data and territorial information (digital elevation model, basic soil and vegetation parameters).

If more detailed territorial information is available the parameterization methodology can be approached reducing the number of assumptions and linking the parameters more tightly to territorial characteristics.

The sensitivity analysis has been carried out on five parameters: two parameters regulate the overland flow, the shape of the hydrograph and response time, two parameters are related to the soil characteristics and affects infiltration and relative soil humidity, and one parameter that takes into account soil porosity and the ratio between vertical and horizontal saturated soil conductivity.

Calibration and validation have been carried out on different periods with reference to two different outlet sections of Orba basin, with different characteristics in terms of soil use, slope and response time. The model produces good results in terms of discharge for both outlet sections.

Model initialization is a hard issue and influences the simulation for quite a long period; in particular the definition of initial water table level is a sensitive challenge. The ideal situation is to extend as far as possible the warm-up period, including a long period without rainfall events. The water table initialization methodology here is based on a possible spatial distribution of water table that exploits morphological constraints (Hjerdt et al., 2004). The method tends to reduce the influence in time of the initial state on discharge simulation as demonstrated in the analysis. For both calibration

HESSD
9, 7639–7697, 2012

and validation, the starting time of the simulations has been chosen about five months before the beginning of the period of analysis.

Further validation analysis has been carried out comparing LST estimated by the model and satellite measurements at both pixel and basin scale. The results provide evidence that Continuum reliably models the LST dynamics at various temporal scales, with some periods of overestimation, particularly during the warmer hours of summer. During the cold season the modeled LST has a lower variability respect to the satellite estimates, but here the percentage of reliable data is quite scarce because of the more frequent cloud covering, and this makes more uncertain the comparison.

The LST comparison showed potential for additional constraints to be used in the calibration phase or to be exploited in a more comprehensive assimilation framework. The distributed nature of the LST in comparison to traditional calibration time series (e.g. discharge data series) would add important information for a better estimation of state variables and parameter patterns.

The approach followed in the design of Continuum proposes to concentrate the efforts in augmenting the number of state variables that are predicted by the model and those that are also observables by using classical or remote instruments of measure. Specific attention is paid to distributed variables (e.g. LST fields) which offer very different information when compared to integral measures (e.g. discharge time series).

Acknowledgements. This work is supported by the Italian Civil Protection Department, and by the Italian Regions of Valle d'Aosta and Liguria. We acknowledge the Italian Civil Protection Department for providing us with the data from the regional meteorological observation networks. A special thanks to Fabio Castelli for his support and his advice.

HESSD

9, 7639–7697, 2012

References

Abbott, M. B., Bathurst, J. C., Cunge, J. A., O'Connell, P. E., and Rasmussen, J.: An introduction to the European Hydrological System – Système Hydrologique Européen, "SHE", 1: history and philosophy of a physically-based, distributed modelling system, J. Hydrol., 87, 45–59, 1986.

Anderson, R. M., Koren, V. I., and Reed, S. M.: Using SSRUGO data to improve Sacramento model a priori parameter estimates, J. Hydrol., 320, 103–116, 2006.

Bartholmes and Todini: Coupling meteorological and hydrological models for flood forecasting, Hydrol. Earth Syst. Sci., 9, 333–346, doi:10.5194/hess-9-333-2005, 2005.

Bauer, S.: A modified Horton equation during intermittent rainfall, Hydrol. Sci. Bull., 19, 219–229, 1974.

Beven, K.: Prophecy reality and uncertainty in distributed hydrological modeling, Adv. Water Resour., 16, 41–45, 1993.

Beven, K.: TOPMODEL: a critique, Hydrol. Process., 11, 1069–1085, 1997.

Beven, K. and Binley, A. M.: The future of distributed models: model calibration and uncertainty prediction, Hydrol. Process., 24, 43–69, 1992.

Beven, K. and Freer, J.: A dynamic TOPMODEL, Hydrol. Process., 15, 1993–2011, 2001.

Bhumralkar, C. M.: Numerical experiments on the computation of ground surface temperature in an atmospheric general circulation model, J. Appl. Meteorol., 14, 1246–1258, 1975.

Blackadar, A. K.: Modeling the nocturnal boundary layer, Proceedings of the Third Symposium on Atmospheric Turbulence, Diffusion and Air Quality, American Meteorological Society, Boston, MA, 46–49, 1976.

Burnash, R. J. C.: The NWS river forecast system-catchment modeling, in: Computer Models of Watershed Hydrology, edited by: Singh, V. J., Water Resources Publications, Highlands Ranch, Colorado, 311–366, 1995.

Burnash, R. J. C., Ferral, R. L., and McGuire, R. A.: A Generalized Streamflow Simulation System: Conceptual Modeling for Digital Computers, Joint Federal-State River Forecast Center, Sacramento, CA, 1973.

Campo, L., Caparrini, F., and Castelli, F.: Use of multi-platform, multi-temporal, remote sensing data for calibration of a distributed hydrological model: an application in the Arno basin, Italy, Hydrol. Process. 20, 2693–2712, 2006.

HESSD
9, 7639–7697, 2012

Caparrini, F. and Castelli, F.: Variational estimation of soil and vegetation turbulent transfer and heat flux parameters from sequences of multisensor imagery, Water Resour. Res., 40, W12515, doi:10.1029/2004WR003358, 2004.
Caparrini, F., Castelli, F., and Entekhabi, D.: Mapping of land atmosphere heat fluxes and surface parameters with remote sensing data, Bound.-Lay. Meteorol., 107, 605–633, 2003.
Caparrini, F., Castelli, F., and Entekhabi, D.: Estimation of surface turbulent fluxes through assimilation of radiometric surface temperature sequences, J. Hydrometeorol., 5, 145–159, 2004.
Castelli, F.: Atmosphere modeling and hydrology prediction uncertainty, in: GNDCI, Proceedings of Workshop on Hydrometeorology: Impacts and Management of Extreme Floods, La Colombella, Perugia, 1779–1794, 1995.
Castelli, F., Menduni, G., and Mazzanti B.: A distributed package for sustainable water management: a case study in the Arno basin, in: The Role of Hydrology in Water Resources Management, Proceedings of a symposium held on the island of Capri, Italy, October 2008, IAHS Publ. 327, 2009.
Chiew, F. and Mc Mahon, T.: Application of the daily rainfall-runoff model MODHYDROLOG to 28 Australian catchments, J. Hydrol., 153, 383–416, 1994.
Chow, V. T.: Open-Channel Hydraulics, McGraw-Hill, New York, xviii + 680 pp. Illus, 1959.
Deardorff, J. W.: Dependence of air-sea transfer coefficients on bulk stability, J. Geophys. Res., 73, 2549–2557, 1968.
Deardorff, J. W.: Efficient prediction of ground surface temperature and moisture with inclusion of a layer of vegetation, J. Geophys. Res., 783, 1889–1903, 1978.
Dickinson, R.: The force-restore method for surface temperature and its generalization, J. Climate, 1, 1086–1097, 1988.
Dickinson, R. E., Henderson-Sellers, A., and Kennedy, P. J.: Biosphere-Atmosphere Transfer Scheme (BATS) Version 1e as Coupled to the NCAR Community Climate Model, National Centre for Atmospheric Research, Boulder, Colorado, NCAR/TN-387+STR, 72 pp., 1993.
Dingman, S.: Physical Hydrology, Prentice-Hall Inc., Englewood Cliffs, NJ, 1994.
Diskin, M. H. and Nazimov, N.: Linear reservoir with feedback regulated inlet as a model for the infiltration process, J. Hydrol., 172, 313–330, 1994.
Downer, C. W., Ogden, F. L., Martin, W. D., and Harmon, R. S.: Theory development and applicability of the surface water hydrologic model CAS 2D, Hydrol. Process., 16, 255–275, 2002.

HESSD
9, 7639–7697, 2012

Dunne, T. and Black, R. D.: An experimental investigation of runoff production in permeable soils, Water Resour. Res., 6, 478–490, 1970.
EUMETSAT: Product user manual, vegetation parameters, http://landsaf.meteo.pt/ (last access: 10 March 2011), 2008.
EUMETSAT: Algorithm Theoretical Basis Document for Land Surface Temperature (LST)., http://landsaf.meteo.pt/ (last access: 22 September 2011), 2009.
Freitas, S. C., Trigo, I. F., Bioucas-Dias, J. M., and Gottsche, F. M.: Quantify the uncertainty of land surface temperature retrievals from SEVIRI/Meteosat, IEEE T. Geosci. Remote, 45, 523–534, 2010.
Gabellani, S., Silvestro, F., Rudari, R., and Boni, G.: General calibration methodology for a combined Horton-SCS infiltration scheme in flash flood modeling, Nat. Hazards Earth Syst. Sci., 8, 1317–1327, doi:10.5194/nhess-8-1317-2008, 2008.
Garrote, L. and Bras, R. L.: A distributed model for real-time forecasting using digital elevation models, J. Hydrol., 167, 279–306, 1995.
Giannoni, F., Roth., G., and Rudari, R.: A semi-distributed rainfall-runoff model based on a geomorphologic approach, Phys. Chem. Earth, 25, 665–671, 2000.
Giannoni, F., Roth., G., and Rudari, R.: Can the behavior of different basins be described by the same model's parameter set? A geomorphologic framework, Phys. Chem. Earth, 28, 289–295, 2003.
Giannoni, F., Roth., G., and Rudari, R.: A procedure for drainage network identification from geomorphology and its application to the prediction of the hydrologic response, Adv. Water Resour., 28, 567–581, 2005.
Hijerdt, K. N., McDonnell, J. J, Seibert, J., and Rodhe, A.: A new topographic index to quantify downslope controls on local drainage, Water Resour. Res., 40, W05602, doi:10.1029/2004WR003130, 2004.
Hu, Z. and Islam, S.: Prediction of ground surface temperature and soil moisture content by the force restore method, Water Resour. Res., 31, 2531–2539, 1995.
Julien, P. Y., Saghafian, B., and Ogden, F. L.: Raster-based hydrologic modeling of spatially-varied surface runoff, Water Resour. Bull., AWRA, 31, 523–536, 1995.
Karsten, J., Gurtz, J., and Lang, H.: Advanced flood forecasting in Alpine watersheds by coupling meteorological observations and forecasts with a distributed hydrological model, J. Hydrol., 267, 40–52, 2002.

HESSD
9, 7639–7697, 2012

Kozak, J. A., Ahuja, L. R., Green, T. R., and Ma, L.: Modelling crop canopy and residue rainfall interception effects on soil hydrological components for semi-arid agriculture, Hydrol. Process. 21, 229–241, 2007.
Kumar, S. V., Reichle, R. H., Peters-Lidard, C. D., Koster, R. D., Zhan, X., Crow, W. T., Eylander, J. B., and Houser, P. R.: A land surface data assimilation framework using the land information system: description and applications, Adv. Water Resour., 31, 1419–1432, 2008.
Legates, D. R. and McCabe, G. J.: Evaluating the use of "goodness-of-fit" measures in hydrologic and hydroclimatic model validation, Water Resour. Res., 35, 233–241, 1999.
Lin, J. D.: On the force-restore method for prediction of ground surface temperature, J. Geophys. Res., 85, 3251–3254, 1980.
Liu, Z., Martina, M. L. V., and Todini, E.: Flood forecasting using a fully distributed model: application of the TOPKAPI model to the Upper Xixian Catchment, Hydrol. Earth Syst. Sci., 9, 347–364, doi:10.5194/hess-9-347-2005, 2005.
Madsen, H.: Automatic calibration of a conceptual rainfall-runoff model using multiple objectives, J. Hydrol., 235, 276–288, 2000.
Maidment, D.: Handbook of Hydrology, McGraw-Hill Inc., 1992.
Marchi, E. and Rubatta, A.: Meccanica dei fluidi, Principi ed applicazioni, UTET, Torino, 1981.
Middelkoop, H., Daamen, K., Gellens, D., Grabs, W., Kwadijk, J. C. J., Hang, H., Parmet, B. W. A. H., Schädler, B., Schulla, J., and Wilke, K.: Impact of Climate Change on Hydrological Regimes and Water Resources Management in the Rhine Basin, Climatic Change, 49, 105–128, 2001.
Mishra, S. and Singh, V.: Soil Conservation Service Curve Number (SCS-CN) Methodology, Kluwer Academic Publisher, 2003.
Nash, J. E. and Sutcliffe, J. V.: River flood forecasting through conceptual models I: a discussion of principles, J. Hydrol., 10, 282–290, 1970.
Noihan, J. and Planton, S.: Simple parameterization of land surface processes for meteorological models, Mon. Weather Rev., 117, 536–549, 1989.
Peters, C. D., Blackburn, E., Liang, X., and Wood, E. F.: The effect of soil thermal conductivity parameterization on surface energy fluxes and temperature, Water Resour. Prog., 55, 1209–1224, 1997.
Rey, J. M.: Modeling potential evapotranspiration of potential vegetation, Ecol. Model., 123, 141–159, 1999.

HESSD
9, 7639–7697, 2012

Rigon, R., Bertoldi, G., and Over, T. M., Geotop: a distributed hydrological model with coupled water and energy budgets, J. Hydrometeorol., 7, 371–388, 2006.
Risse, L., Liu, B., and Nearing, M.: Using curve number to determine baseline values of green-ampt effective hydraulic conductivities, Water Resour. Bull., 31, 147–158, 1995.
Saulnier, G. M., Beven, K., and Obled, C.: Including spatially variable effective soil depths in TOPMODEL, J. Hydrol., 202, 158–172, 1997.
Savenije, H. H. G.: Equifinality, a blessing in disguise?, Hydrol. Process., 15, 2835–2838, 2001.
Schlosser, C. A., Speranskaya, N. A., Robock, A., Vinnikov, K. Y., and Xue, Y.: 18-year land-surface hydrology model simulations for a midlatitude grassland catchment in Valdai, Russia, Mon. Weather Rev., 125, 3279–3296, 1997.
Todini, E. and Ciarapica, L.: The TOPKAPI Model, Mathematical Models of Large Watershed Hydrology, in: Water Resources Publications, Chapter 12, edited by: Singh, V. P. and Frevert, D. K., Littleton, Colorado, 2001.
Wang, J., Endreny, T. A., and Hassett, J. M.: Power function of hydraulic conductivity for a TOPMODEL-based infiltration routine, Hydrol. Process., 20, 3825–3834, 2006.
Winchell, M., Gupta, H. V., and Sorooshian, S.: On the simulation of infiltration- and saturation-excess runoff using radar based rainfall estimates: effect of algorithm uncertainty and pixel aggregation, Water Resour. Res., 34, 2655–2670, 1998.
Winsemius, H. C., Savenije, H. H. G., Gerrits, A. M. J., Zapreeva, E. A., and Klees, R.: Comparison of two model approaches in the Zambezi river basin with regard to model reliability and identifiability, Hydrol. Earth Syst. Sci., 10, 339–352, doi:10.5194/hess-10-339-2006, 2006.
Wooding, R. A.: A hydraulic modeling of the catchment-stream problem, 1. Kinematic wave theory, J. Hydrol., 3, 254–267, 1965.
Zhao, C.: Potential Vegetation Modeling with Variable Leaf Area Index in Semi-arid Grassland of Loess Plateau, China, Proceeding of Geoscience and Remote Sensing Symposium, IEEE, 5, 3311–3313, 2003.

HESSD
9, 7639–7697, 2012

Table 1. Summary of the model parameters that need calibration with their brief description.

Parameter	Description
u_h (s^{-1})	Flow motion coefficient in hillslopes
u_c ($m^{0.5} s^{-1}$)	Friction coefficient in channels
c_f (–)	Defines the infiltration capacity at saturation
c_t (–)	Defines the mean field capacity
R_f (–)	Related to anisotropy between the vertical and horizontal saturated conductivity, and to soil porosity
V_{Wmax} (mm)	Maximum water capacity of the aquifer on the whole investigated area

HESSD
9, 7639–7697, 2012

Table 2. Set of parameters obtained by the calibration.

Parameter	R_f (–)	c_f (–)	c_t (–)	u_h (s^{-1})	u_c ($m^{0.5}\,s^{-1}$)
Calibrated value	1	0.02	0.52	5×10^{-2}	29

HESSD
9, 7639–7697, 2012

Table 3. Values of skill estimators for the whole calibration period.

Outlet Section	RMSE ($m^3 s^{-1}$)	Nash Sutcliffe (–)	Chiew and McMahon (–)	CORR (–)
Casalcermelli	1.84	0.89	0.85	0.95
Tiglieto	1.62	0.70	0.76	0.90

HESSD
9, 7639–7697, 2012

Table 4. Values of percentage error for the peak flows (PPE) of the main events occurred during the calibration.

Event Date	Casalcermelli PPE (%)	Tiglieto PPE (%)
16 Aug 2006	27	7
14 Sep 2006	8	13
25 Sep 2006	−2.3	−17
23 Oct 2006	41	4
17 Nov 2006	−40	−42
9 Dec 2006	−26	2

HESSD
9, 7639–7697, 2012

Table 5. Values of skill estimators for the whole validation period.

Outlet Section	RMSE ($m^3 s^{-1}$)	Nash Sutcliffe (–)	Chiew and McMahon (–)	CORR (–)
Casalcermelli	1.06	0.91	0.89	0.96
Tiglieto	0.83	0.80	0.83	0.91

HESSD
9, 7639–7697, 2012

Table 6. Values of percentage error for the peak flows (PPE) of the main events occurred during the validation period.

Event date	Casalcermelli PPE (%)	Tiglieto PPE (%)
9 Oct 2009	78	21
2 Nov 2009	48	21
8 Nov 2009	−12	20
30 Nov 2009	−10	−15
24 Dec 2009	−25	−11

HESSD
9, 7639–7697, 2012

Table 7. Comparison of satellite estimates and simulated LST. Values of the skill estimators for the period: mean bias (BIAS), root mean square error (RMSE), mean absolute error (AE) and correlation coefficient (CORR).

Target Area	RMSE (˚C)	BIAS (˚C)	MAE (˚C)	CORR (–)
Basin	3.69	0.24	2.27	0.96
Mountain pixel	5.53	2.09	2.88	0.94
Hill pixel	2.01	0.74	2.65	0.96
Flat pixel	2.94	1.08	2.24	0.96

HESSD
9, 7639–7697, 2012

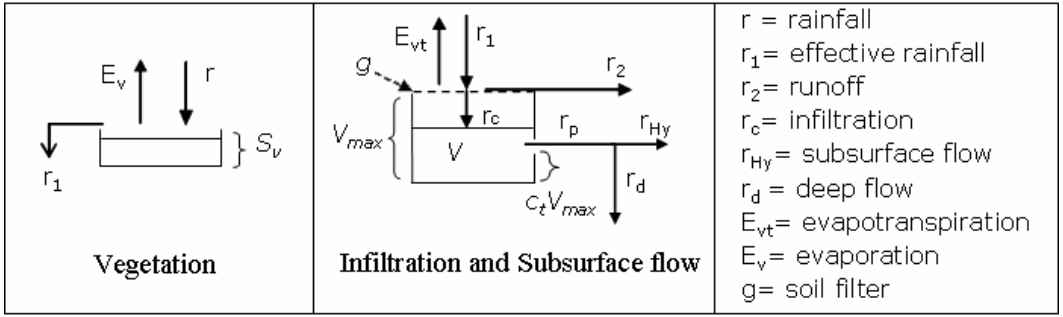

Fig. 1. Sketches of vegetation retention and subsurface flow at cell scale. S_v is the capacity of the vegetation reservoir, V_{max} is the capacity of the soil reservoir, V is the actual water volume in the soil and $c_t V_{max}$ the field capacity of the soil.

HESSD
9, 7639–7697, 2012

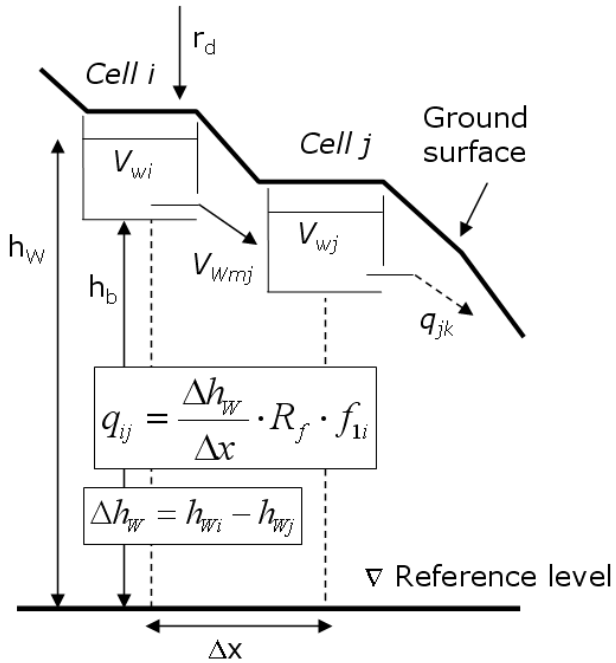

Fig. 2. Sketch of water table flow. As an example two consecutive cells have been considered. The flow is calculated using the water table gradient between the cells. r_d is the deep flow, V_W is the water table actual water content, V_{Wm} is the water table maximum water content, h_W is the absolute level of water table, h_b is the absolute level of impermeable soil layer, R_f a model parameter and Δx the model spatial resolution.

HESSD
9, 7639–7697, 2012

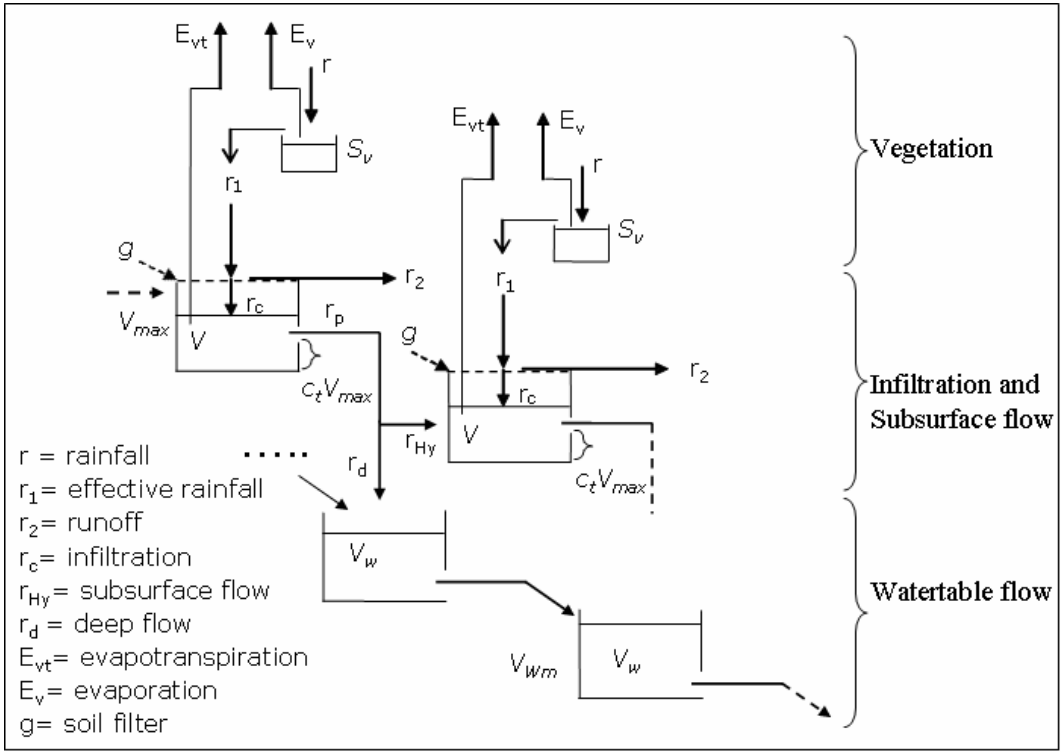

Fig. 3. Sketch of fluxes partition in the Continuum model with the integration of the single modules. Two consecutive cells are illustrated.

HESSD
9, 7639–7697, 2012

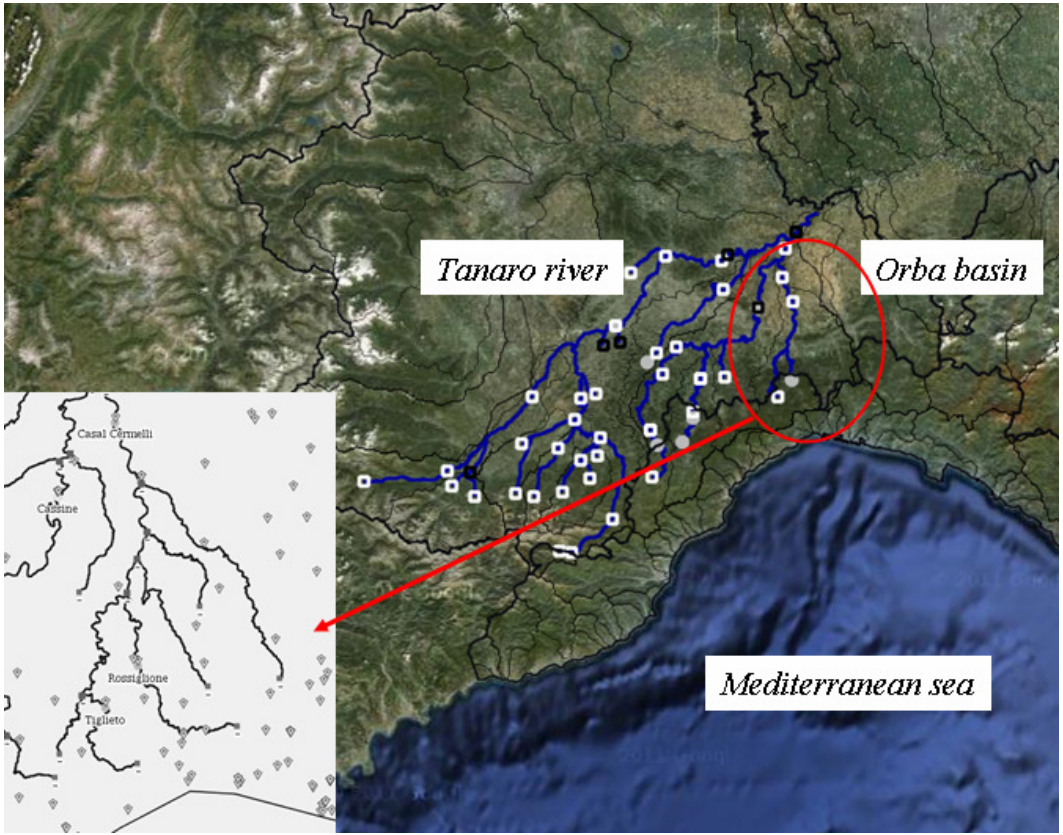

Fig. 4. Orba River location in North-West Italy. On the lower-left corner a zoom on the basin with the micro-meteorological stations. White squares represent the level gauges with rating curve black squares the level gauges without rating curve.

HESSD
9, 7639–7697, 2012

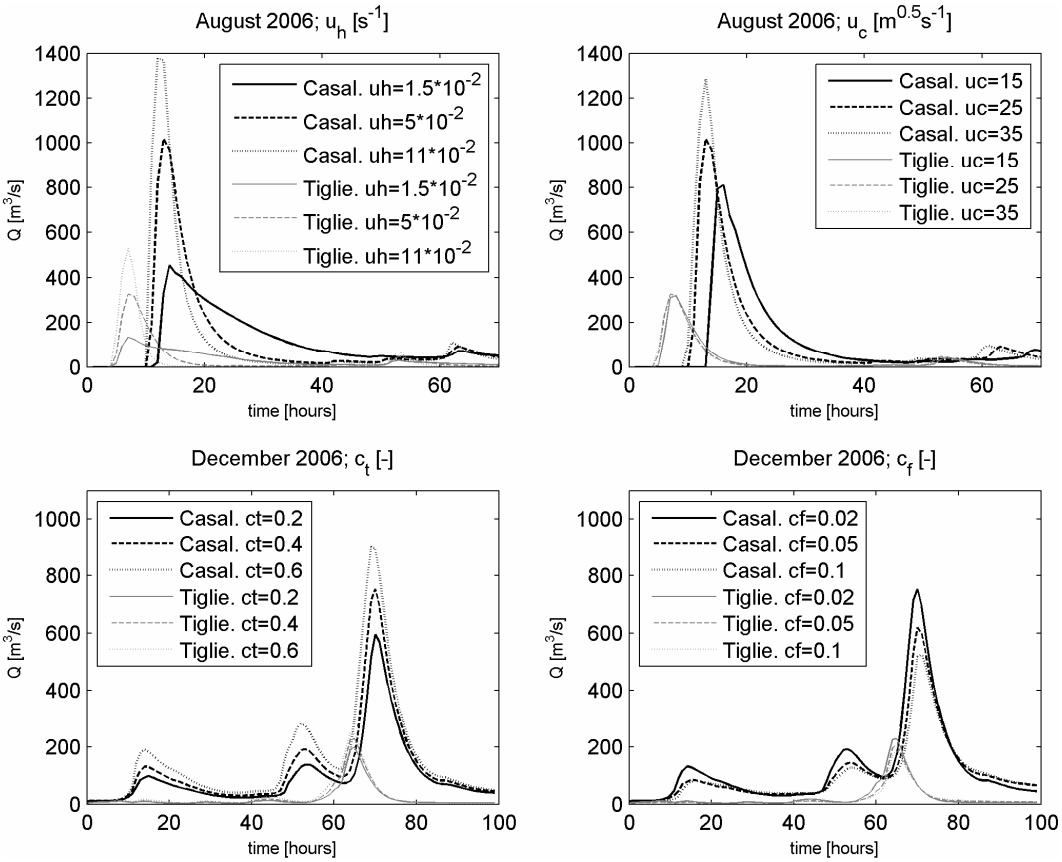

Fig. 5. Sensitivity analysis of the calibration parameters. c_t and c_f are the subsurface flow parameters while u_h and u_c are the overland and channel flow equations parameters.

HESSD
9, 7639–7697, 2012

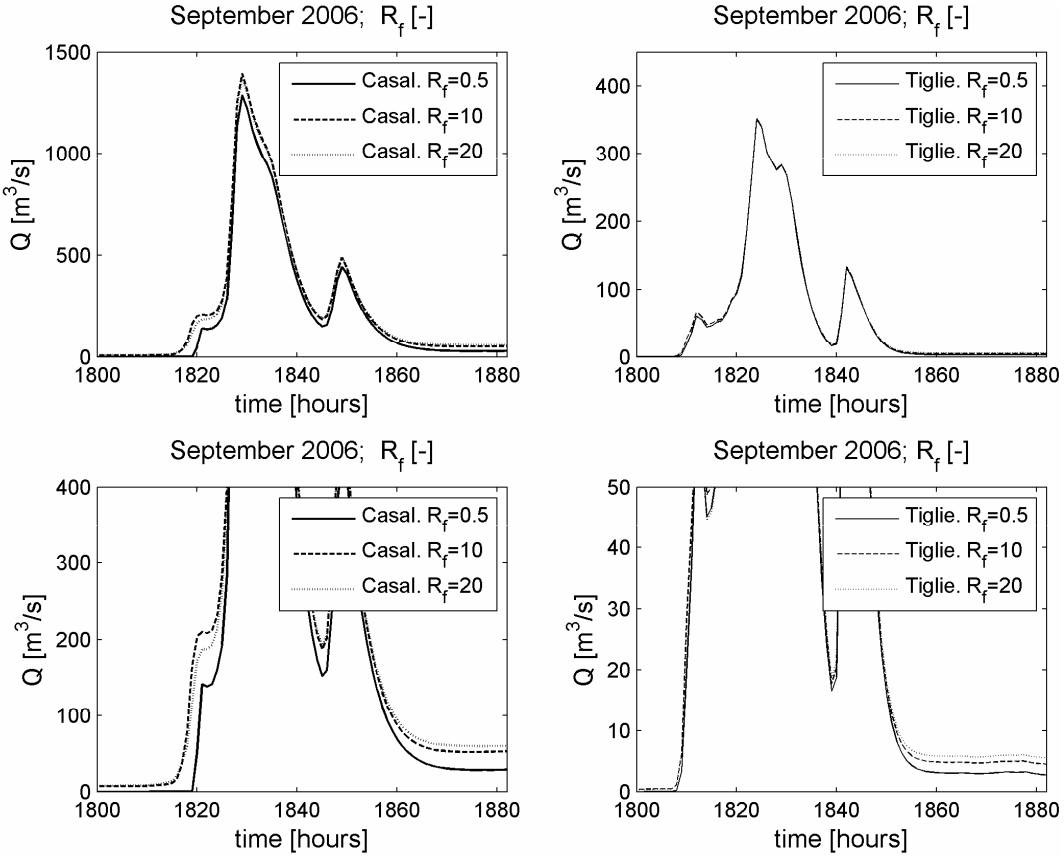

Fig. 6. Sensitivity analysis of the parameter R_f for the two considered outlet sections. The same period is shown with different y axis scales to highlight the differences for both high and low flows.

HESSD
9, 7639–7697, 2012

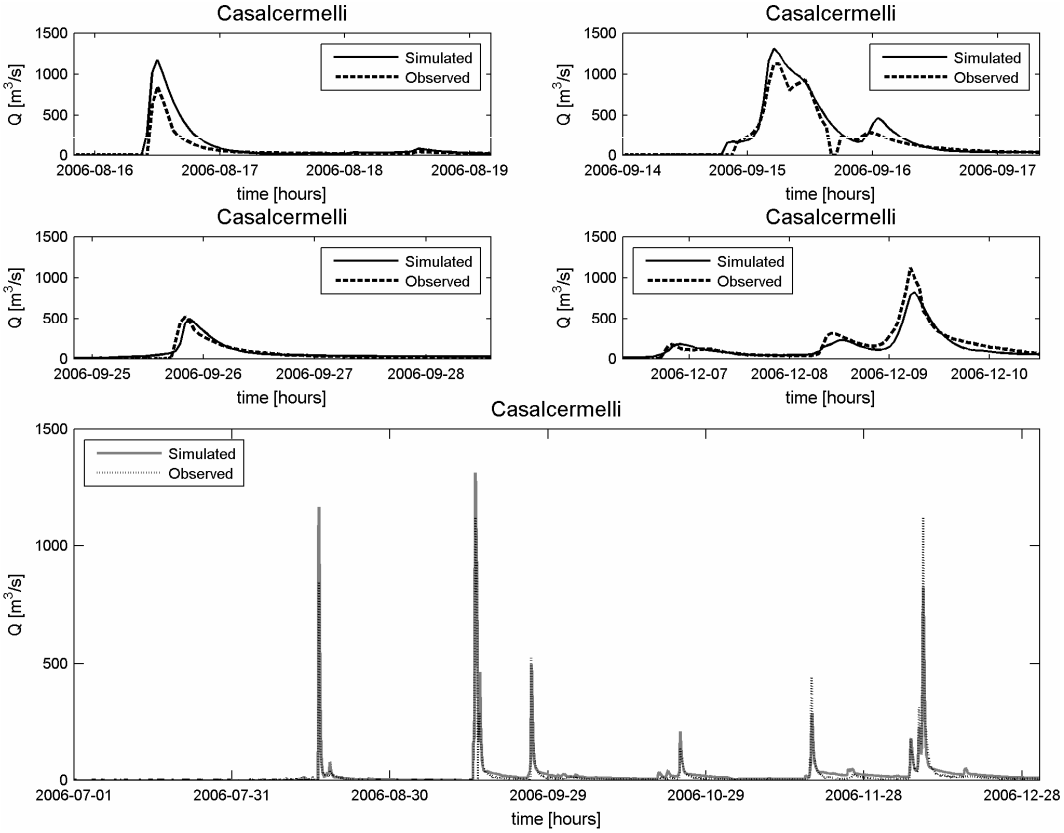

Fig. 7. Comparison between observed and simulated hydrographs for the calibration period. Casalcermelli outlet section.

HESSD
9, 7639–7697, 2012

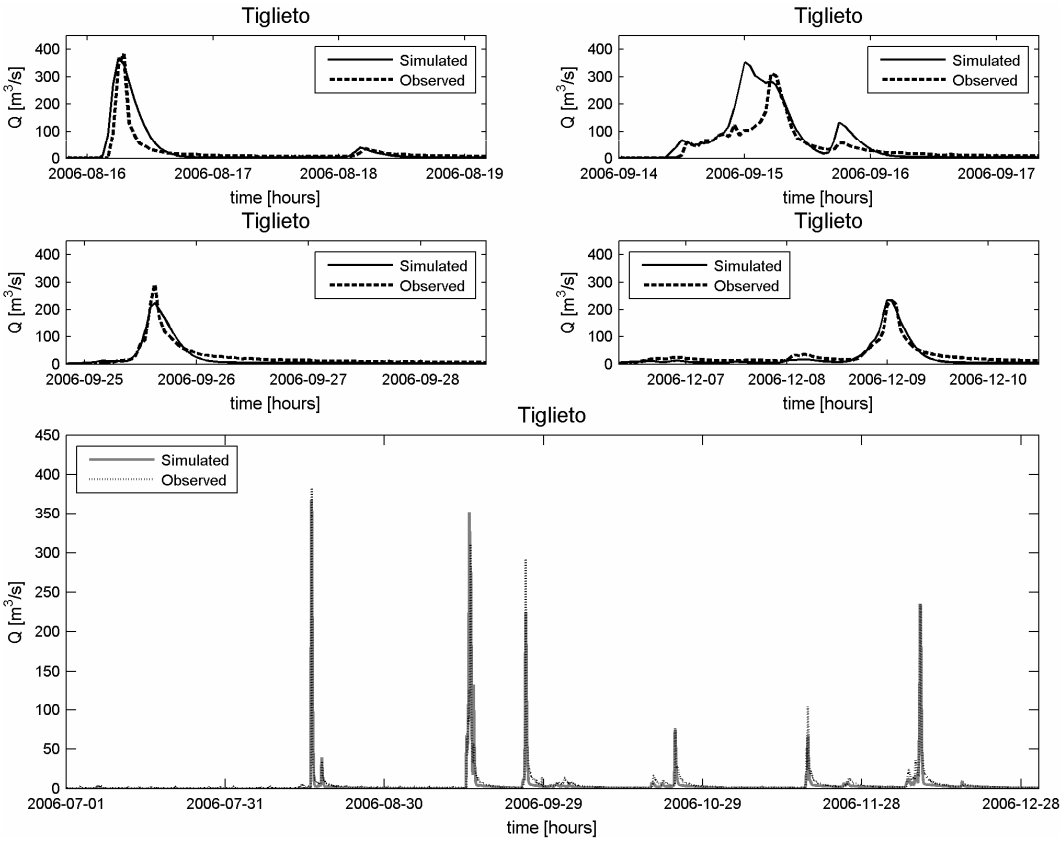

Fig. 8. Comparison between observed and simulated hydrographs for the calibration period. Tiglieto outlet section.

HESSD
9, 7639–7697, 2012

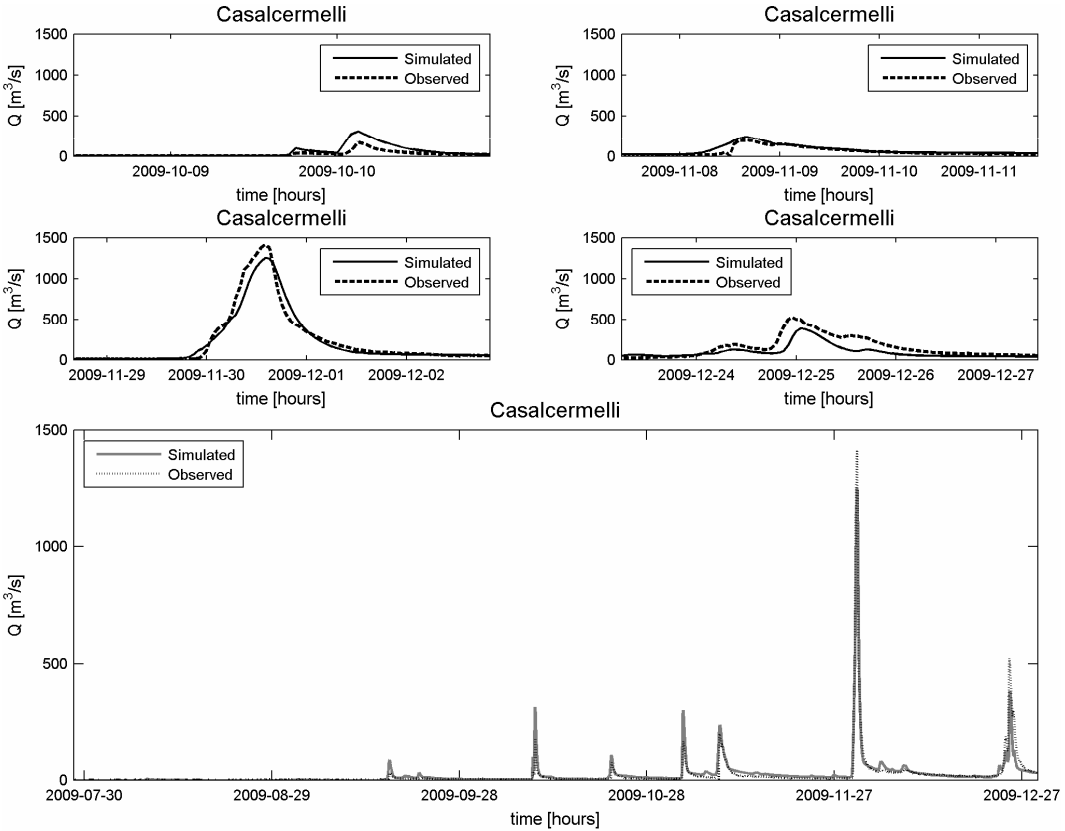

Fig. 9. Comparison between observed and simulated hydrographs for the validation period. Casalcermelli outlet section.

HESSD
9, 7639–7697, 2012

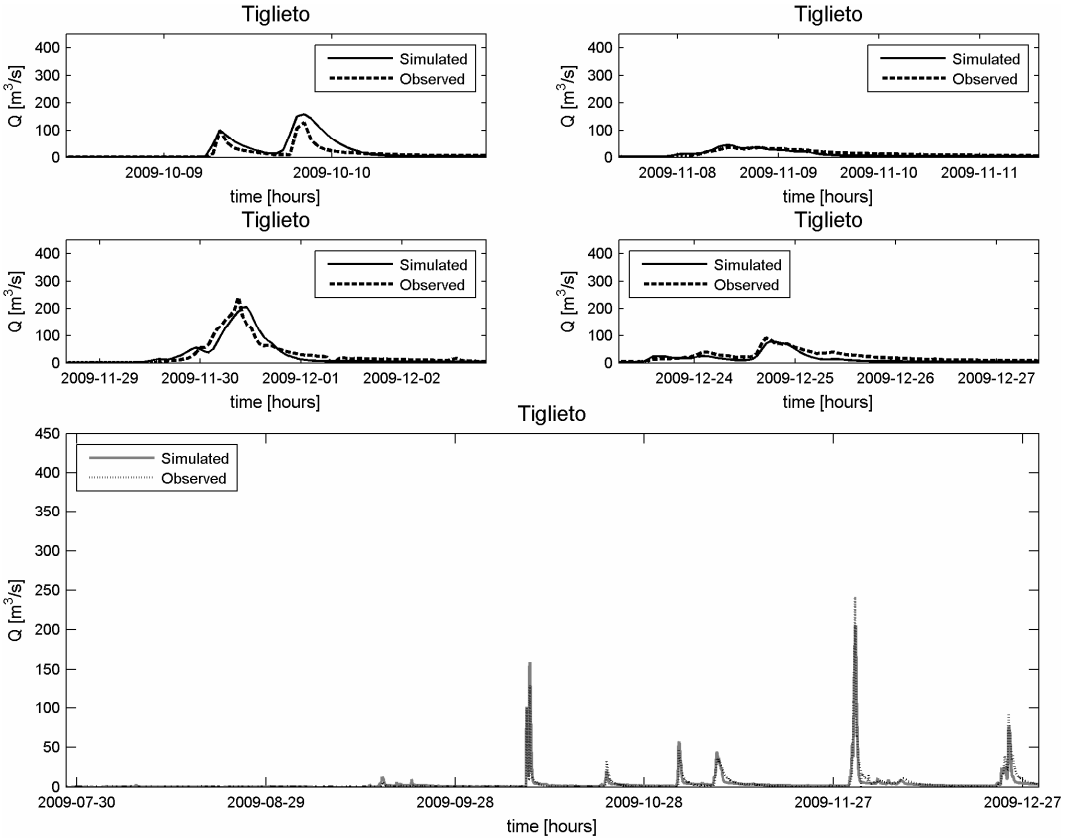

Fig. 10. Comparison between observed and simulated hydrographs for the validation period. Tiglieto outlet section.

HESSD
9, 7639–7697, 2012

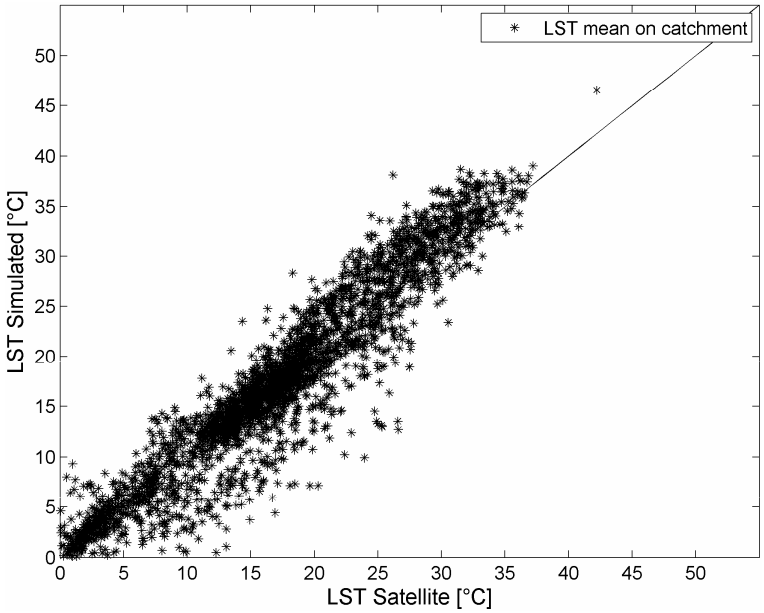

Fig. 11. Comparison between satellite estimates and simulated LST. Average LST at basin scale. The graph refers to the period from 1 June to 31 December 2009.

HESSD
9, 7639–7697, 2012

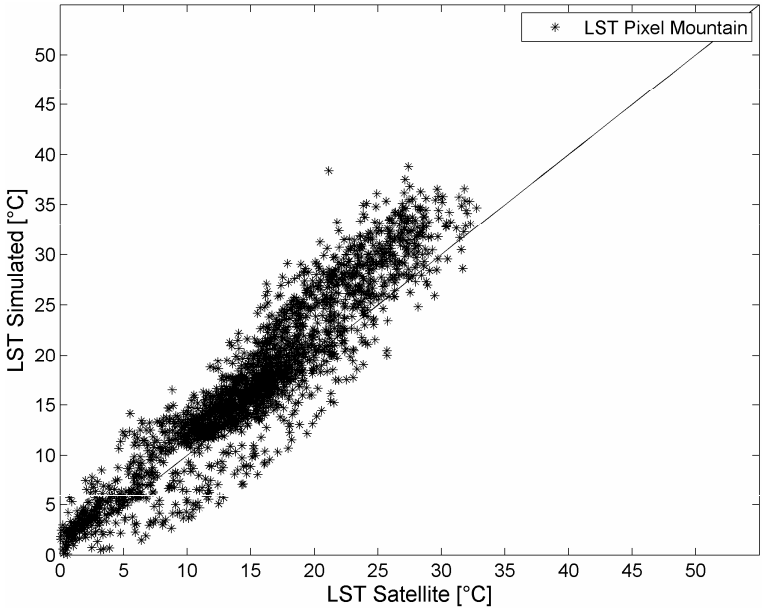

Fig. 12. Comparison between satellite estimates and simulated LST, Mountain Pixel. Graph refers to the period from 1 June to 31 December 2009.

HESSD
9, 7639–7697, 2012

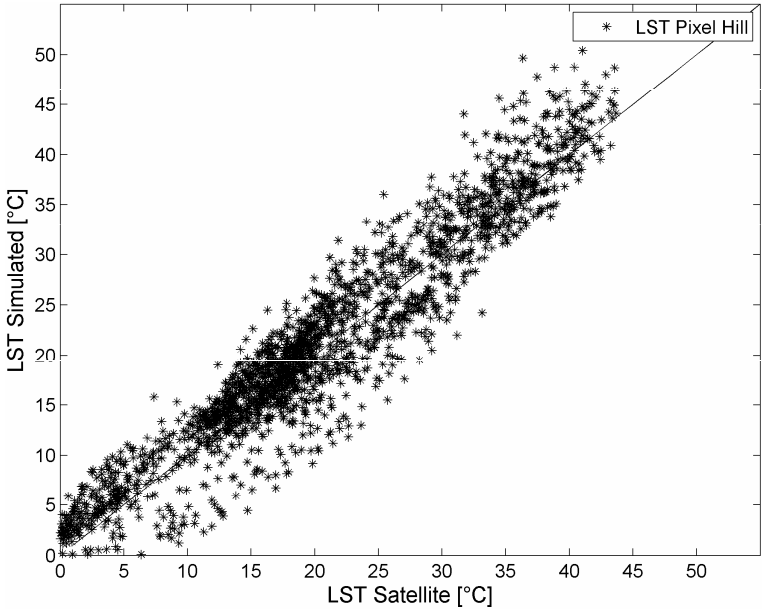

Fig. 13. Comparison between satellite estimates and simulated LST, Hill Pixel. Graph refers to the period from 1 June to 31 December 2009.

HESSD
9, 7639–7697, 2012

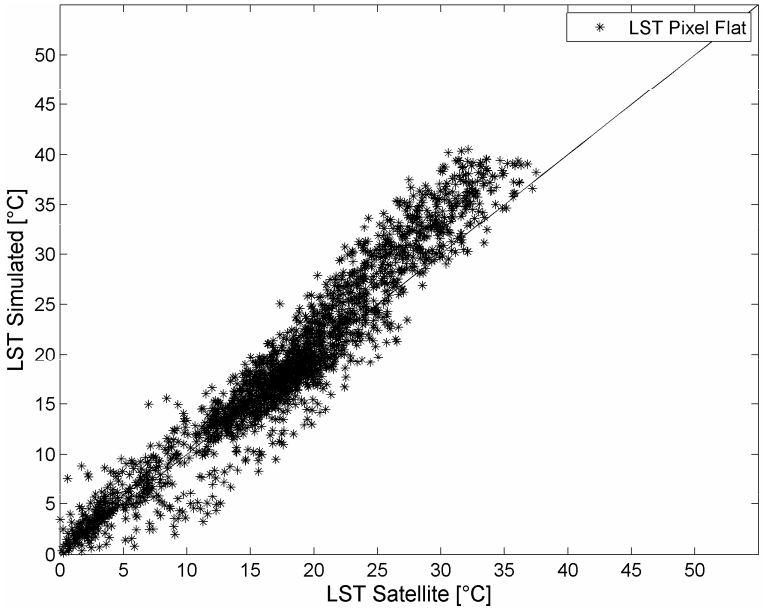

Fig. 14. Comparison between satellite estimates and simulated LST, Flat Pixel. Graph refers to the period from 1 June to 31 December 2009.

HESSD
9, 7639–7697, 2012

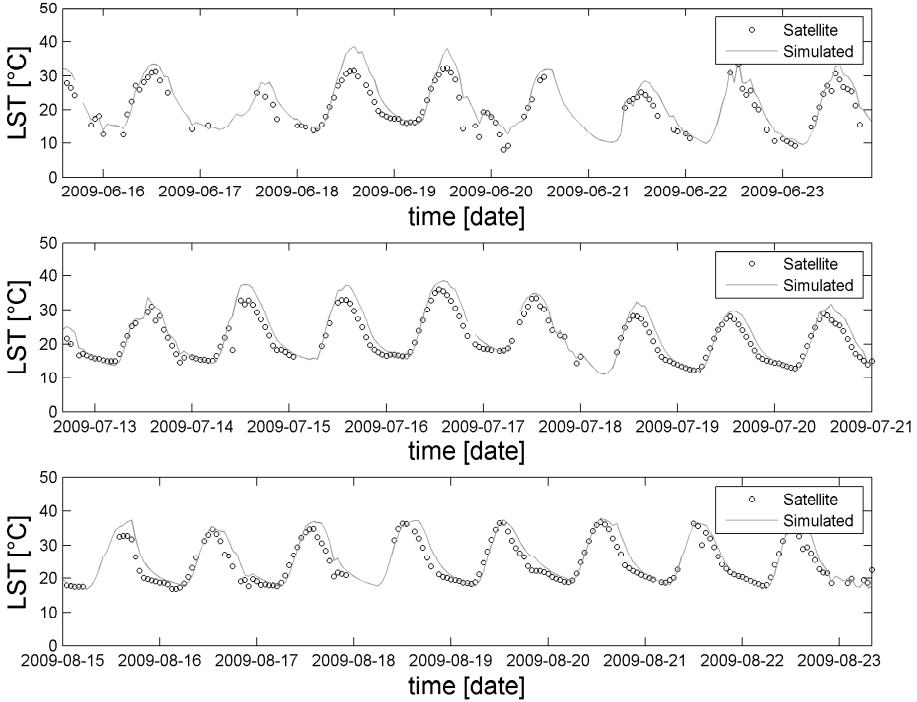

Fig. 15. Comparison between satellite estimates and simulated LST for three periods belonging to the validation period: from 1 June to 31 December 2009. Average LST at basin scale.

HESSD
9, 7639–7697, 2012

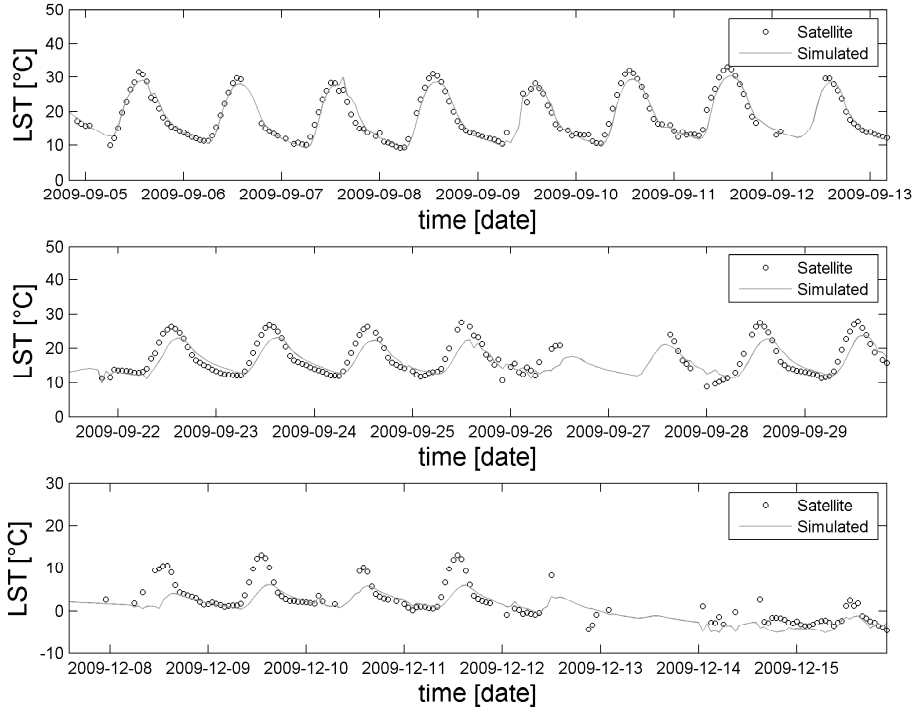

Fig. 16. Same as Fig. 15 but for different sub-periods.

HESSD
9, 7639–7697, 2012

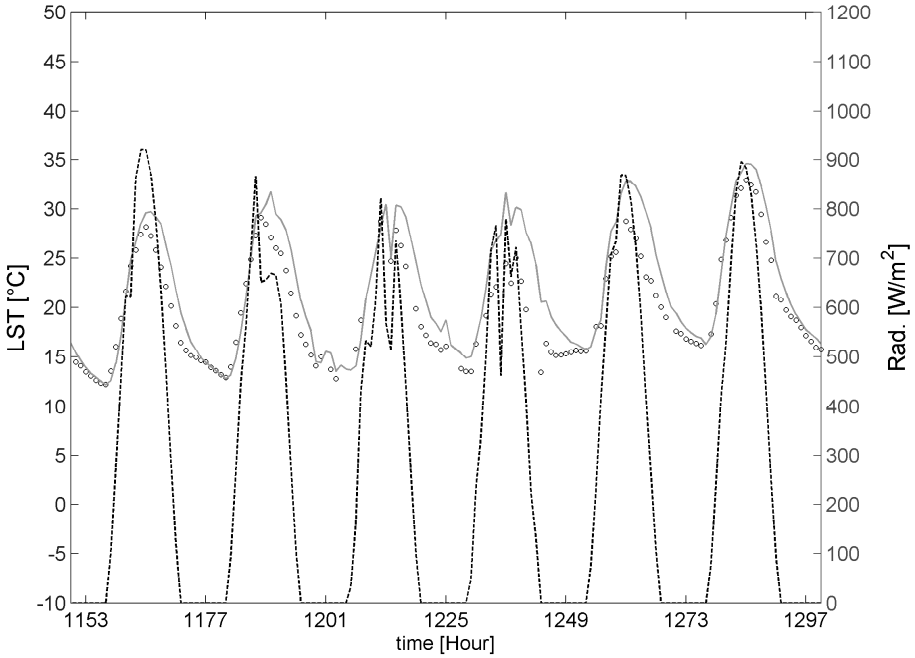

Fig. 17. Simulated (continuous grey line) and satellite estimates (grey circles) LST plotted with observed net radiation (continuous grey black line). The graphs represent the basin scale average values. A brief period of 6 days of June 2009 is shown.

HESSD
9, 7639–7697, 2012

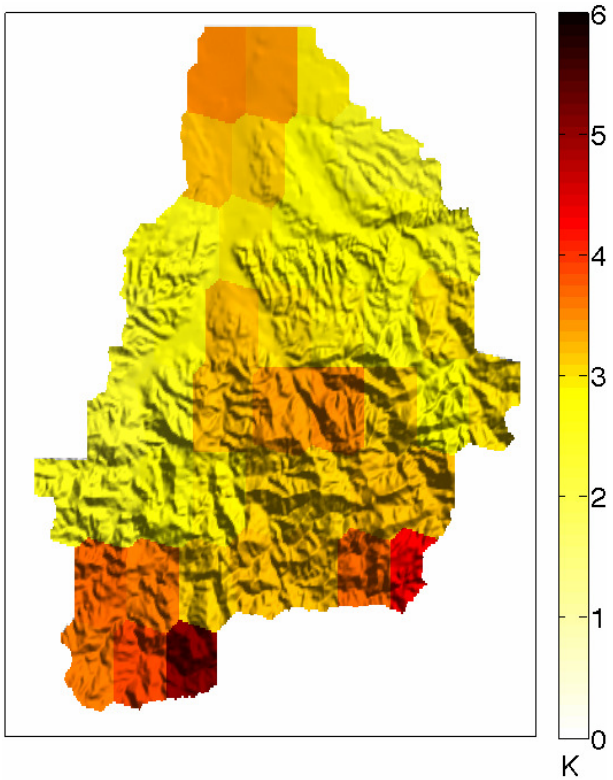

Fig. 18. RMSE map layered over the DEM relief. The value for each pixel is calculated as the mean of the RMSE on the whole validation period.

HESSD
9, 7639–7697, 2012